J. Biomed. Eng. Res.
Vol. 25, No. 3, 183-188, 2004

Magnetic Resonance Imaging of a Current Density Component

Suk Hoon Oh, Tae Seok Park, Jae Yong Han, Soo Yeol Lee[1]

Graduate School of East-West Medical Science, Kyung Hee University, Korea
(Received April 21, 2004. Accepted June 7, 2004)

Abstract : Magnetic resonance current density imaging (MRCDI) is a useful method for measuring electrical current density distribution inside an object. To avoid object rotations during the conventional MRCDI scans, we have reconstructed current density component images by applying a spatial filter to the magnetic field data measured both inside and outside the object. To measure the magnetic field outside the object with MRI, we immersed the object in a water tank. To evaluate accuracy of the current density imaging, we have made a conductivity phantom with a corresponding finite element method model. We have compared the experimentally obtained current density images with the ones calculated by the finite element method. The average errors of the reconstructed current density images were 6.6 ~ 45.4 % when the injected currents were 1 ~ 24 mA. We expect that the current density component imaging technique can be used in diverse biomedical applications such as electrical therapy system developments and biological electrical safety analysis.
Key words : Current density component imaging, MRI, Electrical conductivity, Spatial filter, Electrical safety

INTRODUCTION

Measurement of electrical current densities inside an object is very important in many technical areas such as electric component designs or biomedical equipment developments. Most of the current density measurement techniques measurethe magnetic field first and then calculate the current density from the measured magnetic field data. When measurement of the magnetic field inside the object is not available, highly sensitive magnetic field sensors such as SQUID can be used to measure the magnetic field outside the object [1-4]. The current density inside the object maybe calculated from the externally measured magnetic field data. However, the external magnetic field measurement technique is very prone to errors due to the ill-posedness of the corresponding inverse problem relating the internal current density with the external magnetic field. The external magnetic field measurement technique is now widely used in magnetoencephalogram (MEG) studies and magnetocardiogram (MCG) studies. The magnetic resonance current density imaging (MRCDI) technique measures the magnetic field data inside the object to calculate the current density [5-6]. Since the internal magnetic field data are used in the calculation of the internal current density in MRCDI, MRCDI is much more robust to noise. However, MRCDI suffers from some technical difficulties involved in object rotations during the MRCDI scans. Object rotations are necessary in MRCDI because magnetic resonance imaging (MRI) only sensitizes a single component of the magnetic fieldwhile multiple magnetic field components are necessary for the calculation of the current density. Recently, a new current density image reconstruction method was introduced for MRCDI of a current density component without any object rotations [7]. In the new method, object rotations are not necessary because only a single component data of the magnetic field is used for reconstruction of current density component images.

In this work, we have evaluated performance of MRCDI without object rotations. With a 3.0 Tesla MRI system, we performed MRCDI scans of a conductivity phantom made of sponges and electrolyte to evaluate accuracy of the MRCDI. We also performed finite element method (FEM) analyses to calculate the current densities with the conductivity phantom model. We have compared the experimentally obtained current densities with the ones calculated by FEM. We also present experimental results of MRCDI in biological tissues.

This study was supported by a grant of the Korea Health 21 R&D Project, Ministry of Health and Welfare, Republic of Korea (02-PJ3-PG6-EV07-0002).
통신저자 : Soo Yeol Lee, Graduate School of East-West Medical Science Kyung Hee Univeristy 1 Seochun, Kiheung, Kyungki 449-701, Korea
Tel. +82-31-201-2980 Fax. +82-31-201-3666
E-mail. sylee01@khu.ac.kr

MAGNETIC RESONANCE IMAGING OF A CURRENT DENSITY COMPONENT WITHOUT OBJECT ROTATIONS

When a current density **J** flows inside an object, a magnetic field **B** is produced inside and outside the object. In onventional MRCDI, the formula, $\mathbf{J} = \nabla \times \mathbf{B} / \mu_o$, has been used for the calculation of **J** from the measured magnetic field data **B**, where *mo* is the magnetic permeability in the free space.When we are interested in a component of **J**, for example *Jz*, we need to know two components of **B**, *Bx* and *By*, for the calculation of the current density component. Since MRI sensitizesonly a single component of the magnetic field, two separate MRI scans with an object rotation are necessary for the current density component imaging. When a current density component, for example *Jz*, is dominant,

two magnetic field components, *Bx* and *By*, dominate over the other component *Bz*. Then, the divergence theorem of magnetic field, $\nabla \cdot \boldsymbol{B} = 0$, can be approximated by $\partial B_x / \partial x + \partial B_y / \partial y = 0$. If we represent $\mathbf{J} = \nabla \times \mathbf{B} / \mu_o$ in the spatial frequency domain and substitute the approximated divergence theorem to it, we can obtain the following formula [7],

$$j_z(k_x,k_y)=\frac{i}{\mu_o}\frac{k_x^2+k_y^2}{k_y}b_x(k_x,k_y) \quad (1)$$

where *jz* and *bx*are the Fourier transforms of *Jz* and *Bx*, respectively, *kx* and *ky* are the spatial frequencies in the *x*- and *y*-directions, respectively, and $i = \sqrt{-1}$. Equation (1) implies that a current density component can be reconstructed by applying the spatial filter $\frac{i}{\mu_o}\frac{k_x^2+k_y^2}{k_y}$ to the magnetic field component perpendicular to the current density component. A drawback ofestimating the current density component by equation (1) is that we need to measure a magnetic field component outside the object as well as insidethe object to ensure a sufficient region of support for the Fourier transform. It has been reported that a region of supportof at least four times the object size is necessary in the measurement of the magnetic field component [7]. Since the spatial filter has a high-pass characteristic, the reconstructed current density images are susceptible to the noises appearing in the MRI signals. Therefore, it is desirable to apply an additional filter *h*(*kx*, *ky*) to the spatial filtering to mitigate the noise problem.

$$j_z(k_x,k_y)=\frac{i}{\mu_0}h(k_x,k_y)\frac{k_x^2+k_y^2}{k_y}b_x(k_x,k_y) \quad (2)$$

The magnetic field component can be measured with MRCDI in which current pulses are applied to the object synchronously with the MRI scan [5]. If the current pulse width is *Tc*and the main magnetic field of the MRI system points to the *x*-direction, the extra phase *f* in the magnetic resonance image is given by,

$$\phi(x,y)=\gamma B_x(x,y)T_c \quad (3)$$

where γ is the gyromagnetic ratio of proton (26.75107 rad/Tesla) and *Bx* is the magnetic field component produced by the current pulse.

FEM MODELING OF THE CONDUCTIVITY PHANTOM

To evaluate accuracy of the current density component imaging without object rotations, we have fabricated a conductivity phantom as shown in Fig. 1. The conductivity phantom consists of two sponges immersed in the electrolyte cylinder with the diameter of 50mm. The two sponges have different physical densities. The sponges are in a rectangular cylinder shape of 15mm×30mm×150mm, and they are facing to each other. On the top and bottom of the cylindrical phantom, we placed two metal electrodes to inject electric currents into the phantom. The electrodes were made of copper and the size of the electrodes is 10mm×10mm. The electrolyte was made of distilled water doped with NaCl (3.125 g/l) and CuSO4 (1.0 g/l). The conductivities of the electrolyte (s1) and the two sponges (s2, s3) soaking in the electrolyte were found to be 0.625 S/m, 0.260 S/m, 0.169 S/m, respectively. The conductivities were measured with an impedance analyzer (4192A, Hewlett Packard, USA) at the frequency of 1KHz. At the conductivity measurements, we put the electrolyte or the sponges into a rectangular container and measured the resistance Rbetween the two opposing inner surfaces of the container with two gold coated nickel electrodes. The conductivity s was, then, calculated with the Ohm's law, $R = L/\sigma S$, where L and Sare the length and the cross-sectional area of the container, respectively.

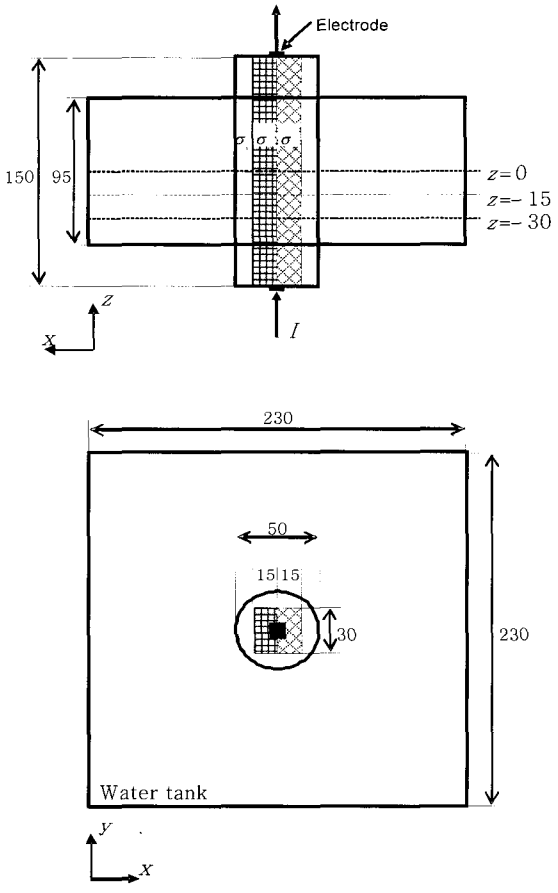

Fig. 1. The conductivity phantom immersed in the water tank. s1, s2 and s3are the conductivities at the electrolyte and sponge regions, respectively.

To compare with the experimental results of the current density component imaging, we made a FEM model of the conductivity phantom. Since we did not apply any fixing structures to the sponges except on the top and bottom of the conductivity phantom not to introduce any conductivity disturbances, it was inevitable for the sponges to deform to some extents. Therefore, we madethe FEM model mimicking the 3-dimensional MRI images of the conductivity phantom. The number of nodes in the FEM model was 74183. For the FEM calculation of the current density, we used a commercial FEM electromagnetic field solver (OPERA, Vectorfields, England). In Fig. 2, we have shown the calculated current densities on z=0 mm. A half region of the conductivity phantom is only shown for the sake of better visualization. The current densities are almost flat in each region and the current densities are almost proportional to the conductivities of the regions. In other planes of z=-15 mm and -30 mm, we observed almost identical current density distribution patterns.

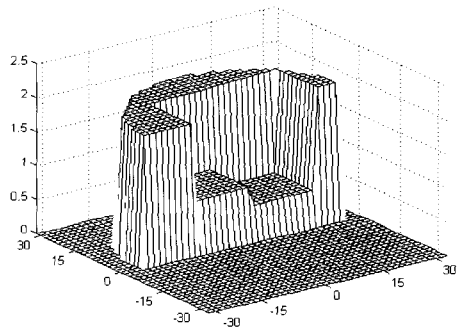

Fig. 2. The calculated current densities on the z=0mm plane. A half region of the conductivity phantom is only shown for the sake of better visualization.

EXPERIMENTAL RESULTS

With the conductivity phantom, we performed MRCDI experiments using a 3.0 Tesla MRI system (Magnum 3.0, Medinus, Korea). To measure the magnetic field outside the phantom, we immersed the phantom in the water tank as shown in Fig. 1. The tank is in a rectangular cylinder shape of 230mm×230mm×95mm. The MRCDI scans were carried out with the spin echo pulse sequence. To avoid electrolysis at the electrodes, the current pulses were applied in a bipolar form. The first half of the bipolar current pulse was positioned between the 90o and 180 oRF pulses and the second half between the 180 o RF pulse and the readout gradient. The repetition time and the echo time were 500 ms and 60 ms, respectively. The imaging matrix size was 256× 256 and the slice thickness was 5mm. The amplitude of the injection currents were controlled between 1 mA and 24 mA with the current pulse width of 40 ms. To prevent fluctuation of the current amplitude due to the electrode aging effect in the electrolyte, we used a current driver operating in the constant current mode. For the MRI signal detection, we used a birdcage RF coil with the diameter of 30cm.

In Fig. 3, we have shown a *Bx* map on *z*=0mm obtained with the injection current of 24 mA. For the phase unwrapping in calculating the *Bx* map from the magnetic resonance phase images, we used the Goldstein's algorithm [8]. Since the outer acryl enclosure of the conductivity phantom (thickness = 1mm) produces no MRI signals, there are phase uncertainties in the enclosure region. Since the enclosure is as thin as about a pixel width, we estimated the phase in the enclosure region with the 2-dimensional median filtering with the filter kernel size of 3×3. By applying the spatial filter to the magnetic field maps, we have obtained the current density component images. We used the Hanning filter to mitigate the noise problem. In Fig. 4, we have shown the reconstructed current density images on *z*=0mm, -15 mm, and -30 mm when the current amplitude was 24 mA. The bright band between the two sponges is due to the uncontrollable gap between the two sponges. Since we used no fixing structures in the two sponges, it was inevitable to allow some deformation of the sponges in the middle of the phantom. In Fig. 5, we have shown the reconstructed current density images on *z*=0mm when the current amplitudes were 3 mA and 12 mA. As the current amplitudes decreases, the current density images become more noisy as expected. In Fig. 6, we have compared the reconstructed current densities with the ones calculated by FEM. The current density values represent the averaged ones over the regions of 9 pixels on *z*=0 mm at the three different regions. The measured conductivity values differ from the calculated ones by 45.4 % at 1 mA, 17.4% at 6 mA, and 6.6 % at 24 mA.

For the current density component imaging in biological tissues, we made a phantom as shown in Fig. 7(a). The phantom consists of ground pig muscle tissues and fat tissues. We used the ground muscle tissues for the sake of convenience in constructing the phantom. For the spin echo MRCDI, we used the repetitiontime of 1500 ms, the echo time of 60 ms and the slice thickness of 5 mm. The current amplitude was 24 mA and the current pulse width was 40 ms. In Fig. 7 (b)and (c), we have shown a magnetic resonance image and a current density component image at the middle of the phantom. We can clearly see the smaller current densities at the fat region. The average current densities are 3.2 mA/cm2 and 0.3mA/cm2 at the muscle and fat regions, respectively. Considering the average conductivity values, 0.05~0.4 S/m and 0.02~0.05 S/m, of the muscle and fat tissues, respectively, and strong conductivity anisotropy of the muscle tissues [9], we think that the measured current density values are quite plausible.

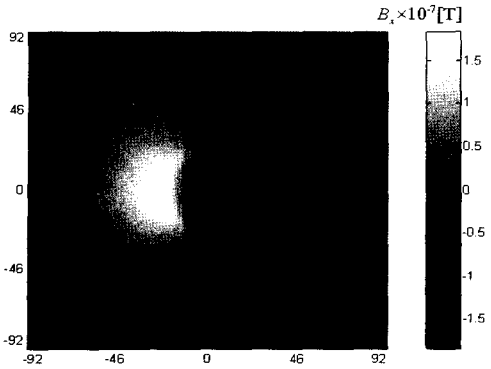

Fig. 3. The Bx map on the z=0mm plane obtained with MRCDI with the injection current of 24 mA.

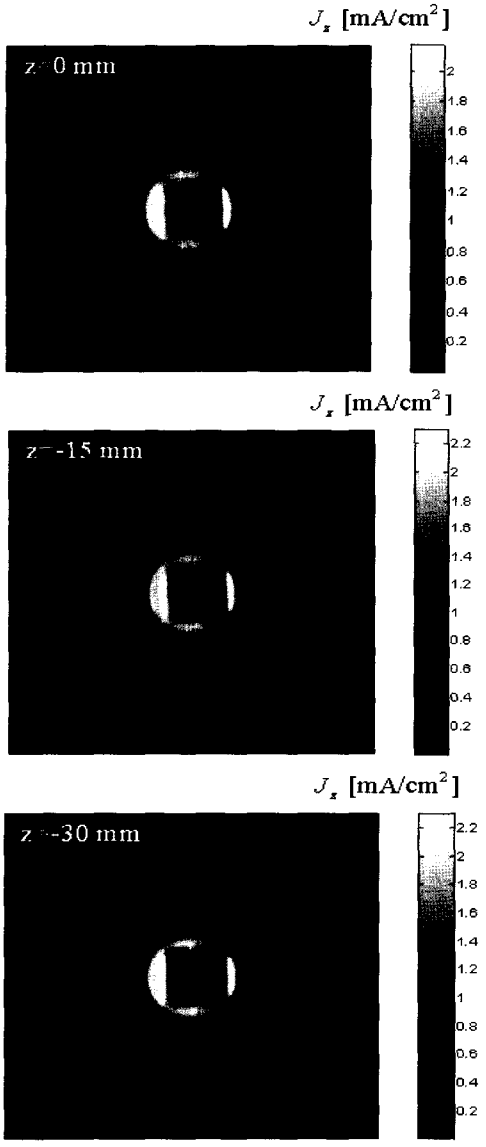

Fig. 4. The reconstructed current densities on z=0mm, -15 mm and -30 mm with the injection current of 24 mA.

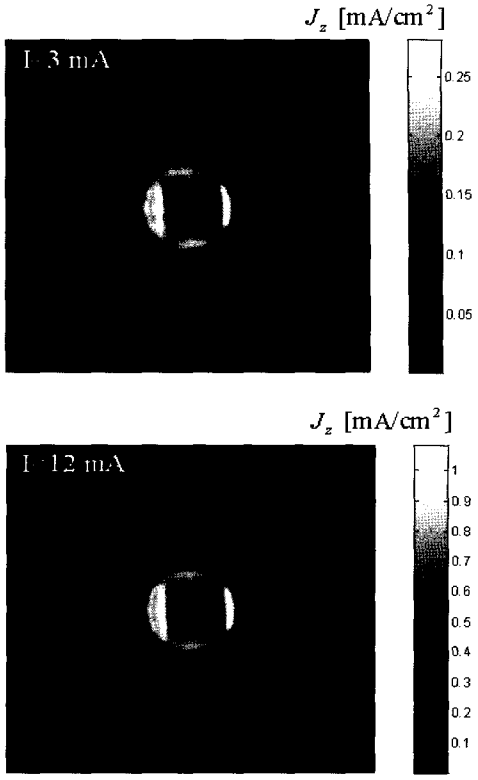

Fig. 5. The reconstructed current densities on z=0mm with the injection currents of 3mA and 12 mA.

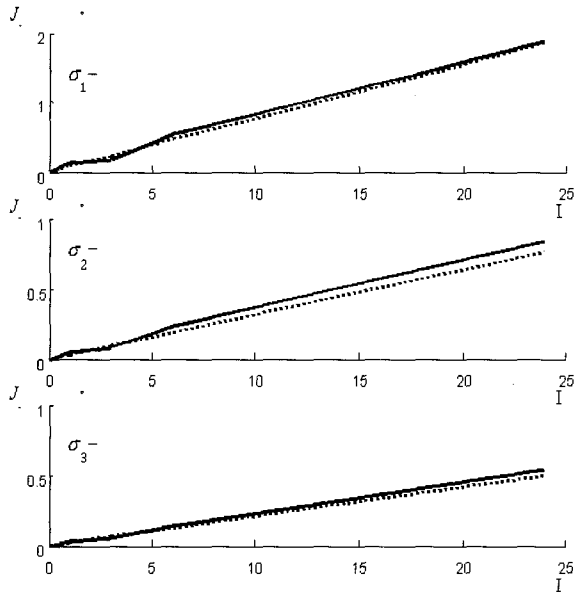

Fig. 6. The current densities obtained with MRCDI (the solid lines) and the current densities calculated by FEM (the dashed lines) in the three different regions with respect to the injection current amplitudes.

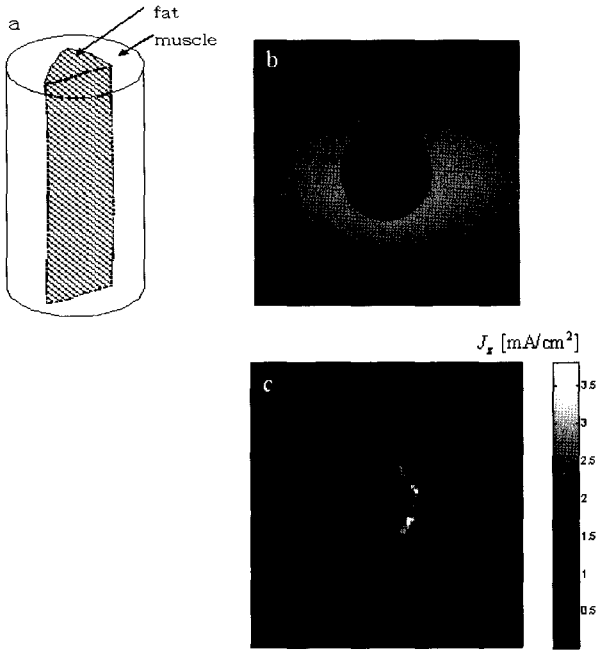

Fig. 7. (a) A schematic diagram of the conductivity phantommade of pig muscle tissues and fat tissues. The same cylinder and water tank as figure 1 are used. (b) A magnetic resonance image of the phantom. (c) The current density image on the cross-sectional plane shown in (b).

DISCUSSIONS AND CONCLUSIONS

Since the MRCDI technique was introduced in 1980's, the MRCDI technique has been limitedly used in the imaging of rigid objects due to the many problems related with the object rotations [10-14]. Especially in biomedical applications, a rotation of soft tissue structures inevitably causes geometrical deformation of the object which in turn makes big errors in the current density calculation. In addition to the geometrical deformation of the object, the object rotations could cause spatial mismatches among the images taken at different rotation anglesdue to the different image distortions. Even if there are no errors in the object rotations, the main field inhomogeneity and the susceptibility effect could cause spatial mismatches which could make big errors in the current density calculation through the curl operation [6].

Since the object rotations are not necessary in the proposed method, it is expected that it can be applied to many biomedical areas. However, the proposed method has two major limitations. Firstly, we have to immerse the object in a liquid tank to measure the magnetic field outside the object. This limits the field of view of the current density images to some extents. If we apply a 256×256 imaging matrix to the magnetic field mapping, the actual matrix size of the current density images is usually smaller than 64×64. Therefore, it is difficult to obtain high spatial resolution images if an imaging matrix as large as 1024×1024 is not available due to the scan time limit or poor signal-to-noise ratio. Secondly, the proposed method is based on the assumption that a single current component is dominant over the other components. In the studies ofbiological tissues consisting mostly of soft tissues, the assumption is almost valid as reported in the previous work [7]. Despite the limitations, we think that we can find many biomedical applications such as electrical safety investigations or electrical therapy system validations. For the biomedical applications, we have to further improve the sensitivity of MRCDI. In the present work, we have obtained current density images with the current amplitude down to 1 mA with the spin echoMRCDI pulse sequence. Since we often use much smaller currents in many biomedical applications, the sensitivity of MRCDI should be further improved. Highly sensitive MRI pulse sequences such as fast spin echo or gradient echo imaging sequence could be considered for MRCDI in the future studies.

In conclusion, the current density component images obtained with MRCDI without object rotations conform to the ones calculated by FEM. However, further studies are still necessary to apply the proposed method to the biomedical field with the currentsless than 1 mA.

REFERENCES

1. Roth BJ et al, "*Using a magnetometer to image a two-dimensional current distribution*", J.Appl. Phys. 65, 361-372, 1989
2. Alvarez RE, "*Biomagnetic Fourier imaging*", IEEE Trans. Med. Imag. 9, 299-304, 1990
3. Kandori A et al, "*Reconstruction of two-dimensional current distribution from tangential MCG measurement*", Phys. Med. Biol. 41, 1705-1716, 1996
4. Zeng XH et al, "*A high-temperature rf SQUID system for magnetocardiography*" , Meas. Sci. Tecnol. 9, 1600-1608, 1998
5. Scott GC et al, "*Measurement of nonuniform current density by magnetic resonance*", IEEE Trans. Med. Imag. 10, 362-374, 1989
6. Scott GC et al, "*Sensitivity of magnetic-resonance current-density imaging*", J. Magn. Reson. 97, 235-254, 1992
7. Oh SH et al, "*A single current density component imaging by MRCDI without subject rotations*", Magn. Reson. Imag. 21, 1023-1028, 2003
8. Ghiglia DC et al, Two dimensional phase unwrapping: Theory, algorithms and software, New York: Wiley Interscience, 1998
9. Grimnes S et al, Bioimpedance & bioelectricity, New York: Academic Press, 2000
10. Beravs K et al, "*Electric current density imaging of bone by MRI*", Magn. Reson. Imag. 15, 909-915, 1997
11. Sersa I et al, "*Electric current density imaging of mice tumors*", Magn. Reson. Med. 37 , 404-409, 1997
12. Gamba HR et al, "*Measurement of electrical current density distribution within the tissues of the head by magnetic*

resonance imaging", Med. Biol. Eng. Comp. 36, 165-770, 1998
13. Yoon RS et al, "*Vector analysis of current pathways in post-mortem pig torso*", Proc. ISMRM 2314, 2002
14. Khang HS et al, "*A preliminary study on temperature change monitoring using the MR current density imaging technique*", Meas. Sci. Technol. 12, N42-N46, 2002